Optimisation of spatially encoded diffusion ordered NMR spectroscopy for the analysis of mixtures

Corentin Jacquemmoz, Rituraj Mishra, Ludmilla Guduff, Carine van Heijenoort, Jean-Nicolas Dumez

Optimisation of spatially encoded diffusion ordered NMR spectroscopy for the analysis of mixtures

Corentin Jacquemmoz,[a] Rituraj Mishra,[a] Ludmilla Guduff,[b] Carine van Heijenoort,[b] Jean-Nicolas Dumez[a]*

a *Université de Nantes, CNRS, CEISAM UMR6230, F-44000 Nantes, France*

b *Université Paris-Saclay, CNRS, ICSN UPR2301, 91190 Gif-sur-Yvette, France*

Abstract

Diffusion-ordered NMR spectroscopy (DOSY NMR) is a widely used method for the analysis of mixtures. It can be used to separate the spectra of a mixture's components, and to analyse interactions. The classic implementation of DOSY experiments, based on an incrementation of the diffusion-encoding gradient area, requires several minutes or more to collect a 2D data set. Spatially encoded (SPEN) DOSY makes it possible to collect a complete data set in less than one second, by spatial parallelisation of the effective gradient area. While several short descriptions of SPEN DOSY experiments have been reported, a thorough characterisation of its features and its practical use is missing, and this hinders the use of the method. Here we present the unusual principles and implementation of the SPEN DOSY experiment, an understanding of which is useful to make optimal use of the method. The encoding and acquisition steps are described, and the parameter relations that govern the setup of SPEN DOSY experiments are discussed. The influence of key parameters, including on sensitivity, is illustrated experimentally on mixtures of small molecules. This study should be useful for the setup of SPEN DOSY experiments, which is particularly useful for systems that evolve in time.

1 Introduction

Nuclear magnetic resonance (NMR) spectroscopy is a powerful tool for the analysis of solution mixtures of small molecules, with applications that include metabolomics and reaction monitoring [1,2]. The diffusion-ordered NMR spectroscopy (DOSY) experiment is particularly well suited for mixture analysis [3,4]. Sometimes referred to as a form of virtual chromatography, it provides separation of the spectra of a mixtures' components, based on their translational diffusion coefficients. The DOSY method is used extensively to help in the identification of a mixtures' components, e.g., for metabolic studies or for authentication application, and to analyse interactions in solution [5].

In DOSY experiments, the diffusion information is encoded by a pair of pulsed-field gradients of duration δ, separated by a delay of duration Δ. Diffusion during the delay results in an attenuation of the acquired signal given by the Stejskal Tanner equation [6]:

$$S(q) = \mathrm{S}_0 e^{-\mathrm{Dq}^2\Delta'}, \tag{1}$$

where S_0 is the initial amplitude of the signal, D is the diffusion coefficient, Δ' is the diffusion delay corrected to account for the finite width of the gradient pulses, and q corresponds to the area of the diffusion-encoding gradient multiplied by the gyromagnetic ratio, and is given by:

$$q = \gamma \int_0^{\delta} G(t')dt', \tag{2}$$

where δ is the duration of the gradient pulses. In practice, a series of 1D experiments are recorded, using an array of values of q. The attenuation of signals as a function of q is fitted to Eq. 1, to yield an estimate of the diffusion coefficient. The consecutive acquisition of multiple 1D spectra, together with the use of phase cycling to enforce coherence transfer pathway selection, results in experiment durations ranging from a few minutes to several hours for classical DOSY experiments. This is a limitation for the analysis of systems that evolve in time, such as reaction media or hyperpolarised substrates.

Several methods have been developed to decrease the duration of DOSY experiments. In the Oneshot approach [7], the need for phase cycling is eliminated by using unbalanced bipolar diffusion encoding gradients. Experiments may then be recorded with a single scan for each value of the diffusion gradient, provided that the equation for the fit is modified to account for the unbalanced gradients. Other approaches aim at reducing the number of values

of *q* needed to estimate diffusion coefficients. For example, accordion or sparse sampling [8,9] of the *q* and indirect time dimension have been used to accelerate 3D DOSY experiments.

Spatial parallelisation is a general approach to accelerate multidimensional NMR experiments, in which several sub-experiments are carried out simultaneously in different slices of the sample [10,11]. Spatial parallelisation of the DOSY experiment was first reported by Loening *et al*., using a z^2 shim coil to create the field variation [12]. A more convenient approach was proposed by Thrippleton *et al.*, based on the joint application of a frequency-swept pulse and a magnetic-field gradient [13]. It was later revisited by Shrot and Frydman [10], who used echo-planar spectroscopic imaging to retrieve the spatially encoded diffusion information for each peak in a more robust manner. Spatial parallelisation is also used in ultrafast Laplace NMR [14–16]. Recently, we have shown that spatially encoded DOSY (SPEN DOSY) could be generalised to higher dimensional experiments [17], and that the acceleration provided by spatial encoding made it possible to collect DOSY data in a single scan for reaction mixtures and hyperpolarised substrates [18–20]. When spatial parallelisation is used, the Stejskal Tanner equation is replaced by [12,13,21,22]:

$$S(z) = \mathrm{S}_0 e^{-\mathrm{D}\left(\mathrm{K(z)}\right)^2 \Delta'}, \qquad (3)$$

where K(z) is a position-dependent effective gradient area multiplied by the gyromagnetic ratio. While several brief descriptions of the SPEN DOSY experiments have been reported, a detailed description of the method and of its features for mixture analysis is missing.

In this article, we give a comprehensive description of SPEN DOSY experiments, and describe how to optimise them for the analysis of solution mixtures. The theory of spatial encoding of diffusion coefficients is summarised first, together with the MRI-based acquisition used in SPEN DOSY. The compensation of convection in SPEN DOSY experiments is also explained, as it plays an important role for applications to reaction monitoring. Using the resulting relations, the choice of pulse sequence parameters is then discussed, in the cases of single-axis and triple-axis gradient probes. The influence of key parameters on signal-to-noise ratio and the estimated diffusion coefficient is demonstrated experimentally, as well as with the use of pure-absorption processing. Together these results provide a guide to the use of SPEN DOSY for applications to the analysis of mixtures.

2 Theory

The classical DOSY experiment consists of the acquisition of a series of 1D spectra, with varying intensities of the diffusion-encoding gradient pair. In the SPEN DOSY experiment, this process

is parallelised spatially, as schematised in Figure 1. DOSY experiments most frequently rely on a stimulated-echo implementation, in which magnetisation is stored along the longitudinal axis during the diffusion delay. Figure 2.a shows a pulse sequence for conventional STE DOSY, and the pulse sequence for SPEN STE DOSY is shown in Figure 2.b. Consider the transverse magnetisation of a small volume element. In both cases, the first diffusion-encoding gradient pulse generates a phase variation for the magnetisation that is fully refocussed by the second diffusion-encoding gradient pulse, while diffusion acts to attenuate the magnetisation's amplitude. Spatial parallelisation requires two main ingredients. First, the diffusion encoding gradient pulses are replaced by the combined application of a frequency-swept pulse and a gradient pulse. Second, a spectroscopic imaging scheme is used during acquisition to record a 1D spatial profile for each peak in the spectrum. These two aspects will be described here. Note that spin-echo versions of the SPEN DOSY experiment are also possible and have been described [19].

2.1. Diffusion encoding

In diffusion NMR experiments, translational diffusion is encoded through the irreversible loss of magnetisation that it causes when there is a variation of the spin phase as a function of position. Consider a volume element with a transverse magnetisation $M_+(z,t)$, in the presence of a linear variation of the spin phase of the form $\phi(z) = kz$. Translational diffusion during a delay τ will mix molecules bearing spins with different phases from neighbouring volume elements, thus reducing the transverse magnetization. This attenuation can be quantified by solving the Bloch-Torrey equation and is given by:

$$|M_+(z,t+\tau)| = |M_+(z,t)|e^{-D\tau k^2}, \quad (4)$$

where *D* is the translational diffusion coefficient. This equation can be written in a more general form for a time-dependent spin phase of the form $\phi(z,t) = k(t)z$, as

$$|M_+(z,t+\tau)| = |M_+(z,t)|e^{-D\int_t^{t+\tau}\left(k(t')\right)^2 dt'}. \quad (5)$$

In the case of a linear phase variation, this attenuation is uniform over the sample. This is the case for conventional DOSY experiment, in which the phase imparted by the gradient pulses is such that:

$$k(t) = -\int_0^t \gamma G(t')dt'. \quad (6)$$

Solving Eq.5 for the conventional DOSY pulse sequence gives the Stejskal Tanner equation (Eq.1).

In the SPEN DOSY experiment, the combined application of a frequency-swept pulse and a magnetic field gradient causes a phase variation that is not linear with respect to position. As a result, diffusion attenuation becomes position dependent, and this is used for spatial parallelisation. In order to describe the SPEN DOSY experiment, Eq.6 needs to be generalized to arbitrary spatial phase variations. In addition, the phase variation caused by the combined application of a frequency swept pulse and a magnetic field gradient needs to be calculated. In the case of non-linear phase variation, the attenuation is given by [12,13,21,22]:

$$|M_+(z,t+\tau)| = |M_+(z,t)|e^{-D\int_t^{t+\tau}\left(K(z,t')\right)^2 dt'}, \quad (7)$$

where $K(z,t)$ is the first derivative of the spin phase with respect to position:

$$K(z,t) = \frac{\partial\phi(z,t)}{\partial z}. \quad (8)$$

Equation 8 is valid provided that the typical diffusion length $l = \sqrt{2D\tau}$ is such that the phase variation experienced by the spins during the diffusion delay is approximately linear [12,22]:

$$\left|\frac{\partial^2\phi(z,t)}{\partial z^2}\right| l^2 \ll 2\pi. \quad (9)$$

The phase variation that results from the combined application of a frequency-swept pulse and a magnetic field gradient can be calculated in several ways. One possibility is to assume that nuclear spins flip instantaneously when their precession frequency is equal to the frequency of the pulse [21,22]. Alternatively, the phase can be calculated by numerical integration of the spin's precession frequency in a frequency-modulated frame [12]. The two possibilities are summarised here.

Consider an ensemble of uncoupled spins of precession frequency ω_i(z), that are submitted to the pulse sequence shown in Figure 2.b. During the first swept refocusing pulse of frequency $\omega_{\mathrm{rf}}(t)$, the spins will flip at a time t_{flip}(z) such that:

$$\omega_{\mathrm{rf}}\left(t_{\mathrm{flip}}(z)\right) = \omega_i(z). \quad (10)$$

The spin phase ϕ_1 during the first pulse is given by:

$$\phi_1(z,t) = \omega_i(z)t \text{ for } t < t_{\mathrm{flip},1} \quad (11)$$

$$\phi_1(z,t) = \omega_i(z)\left(t - 2t_{\mathrm{flip},1}(z)\right) + 2\Phi_{\mathrm{rf}}\left(t_{\mathrm{flip},1}(z)\right) \text{ for } t > t_{\mathrm{flip},1} \quad (12)$$

where $\Phi_{\mathrm{rf}}(t_{\mathrm{flip}})$ is the phase of the RF pulse at the time of the flip. This gives for the derivative of Eq (11):

$$K_1(z,t) = \frac{\partial \omega_i(z)}{\partial z} t \text{ for } t < t_{\mathrm{flip},1}, \tag{13}$$

and for the derivative of Eq (12):

$$K_1(z,t) = \frac{\partial \omega_i(z)}{\partial z}\left(t - 2t_{\mathrm{flip},1}\right) - 2\omega_i(z)\frac{\partial t_{\mathrm{flip},1}(z)}{\partial z} + 2\frac{\partial \Phi_{\mathrm{rf}}(t)}{\partial t}\frac{\partial t_{\mathrm{flip},1}(z)}{\partial z} \text{ for } t > t_{\mathrm{flip},1} \tag{14}$$

which can be simplified as:

$$K_1(z,t) = \frac{\partial \omega_i(z)}{\partial z}\left(t - 2t_{\mathrm{flip},1}\right) \text{ for } t > t_{\mathrm{flip},1} \tag{15}$$

based on the fact that $\frac{\partial \Phi_{\mathrm{rf}}(t)}{\partial t} = \omega_{\mathrm{rf}}(t)$ and on the condition that defines the flip time. Similarly, during the second pulse:

$$K_2(z,t) = K_1(z,t) + \frac{\partial \omega_i(z)}{\partial z} t \text{ for } t < t_{\mathrm{flip},2}, \tag{16}$$

and

$$K_2(z,t) = -K_1(z,t) + \frac{\partial \omega_i(z)}{\partial z}\left(t - 2t_{\mathrm{flip},2}\right) \text{ for } t > t_{\mathrm{flip},2}. \tag{17}$$

The total diffusion attenuation due to the spatial encoding blocks is given by:

$$\frac{S}{S_0} = \exp\left(-D\left(\int_{t_1}^{t_1'}\left(K_1(z,t')\right)^2 dt' + (\Delta - 2T_e)\left(K_1(z,t_1')\right)^2 + \int_{t_2}^{t_2'}\left(K_2(z,t')\right)^2 dt'\right)\right). \tag{18}$$

Where t_1 and t_1' are the start and end time of the first spatial encoding block, and t_2 and t_2' are the start and end time of the second spatial encoding block. The SPEN STE DOSY pulse sequence is usually applied with linearly swept, so-called chirp pulses. In this case the time-dependent frequency is, in a rotating frame of reference:

$$\omega_{\mathrm{rf}}(t) = \omega_{\mathrm{rf}}^0 + R\left(t - t_j\right), \tag{19}$$

where R is the sweep rate, ω_{rf}^0 is the initial frequency offset and t_j the start time of the j^{th} pulse. The spin's precession frequency during the spatial encoding block is given by:

$$\omega_i(z) = \Omega_i - \gamma G_e z, \tag{20}$$

where Ω_i is the chemical shift offset and *G* is the magnetic field gradient. From the condition given in Eq.10, the expression of the flip time is:

$$t_{\mathrm{flip,j}} = t_j + \frac{\Omega_i - \gamma G_e z - \omega_{\mathrm{rf}}^0}{R}. \tag{21}$$

Combining these equations, for a symmetric sweep in the frame of reference ($\omega_{\mathrm{rf}}^{0} = -\frac{RT}{2}$), gives the total diffusion attenuation due to the spatial encoding blocks for the pulse sequence shown in Figure 2.b:

$$\frac{S}{S_0} = \exp\left(-\mathrm{D}(\gamma G_e T_e)^2 \left(\frac{4}{3}T_e + \left(\frac{2z'}{L_S} - 1\right)^2 (\Delta - T_e)\right)\right), \tag{22}$$

where

$$L_S = \frac{RT_e}{\gamma G_e} \tag{23}$$

is the length of the region swept by the pulse, and

$$z' = z + \frac{\Omega_i}{\gamma G_e} \tag{24}$$

is the position corrected to account for the chemical-shift displacement during the pulse. The position dependent diffusion attenuation is thus of the form of Eq. 3 with

$$K(z) = -\gamma G_e T_e \left(\frac{2z'}{L} - 1\right) \tag{25}$$

for the effective gradient area, and $\Delta' = \Delta - T_e$ for the effective diffusion delay. The term $\frac{4}{3}T_e$ in Eq. 22 is a global attenuation that is common to all the slices. It is small, and corresponds to the diffusion attenuation experienced during the spatial encoding blocks for the slice at $z = L_S/2$. For analysis, it can be included in the S_0 term. Figure 3 shows the calculated phase that results from the simultaneous application of a 180° chirp pulse and a magnetic field gradient for an initial transverse magnetisation, together with its tangent at several position, showing how diffusion attenuation will be different in different parts of the sample. The additional gradient of duration T_e is used to cover a larger range of effective gradient area.

Alternatively to the analytical expression based on the assumption of an instantaneous flip of the spins, the effective gradient area can be obtained from a numerical calculation of the spin phase at the end of chirp+gradient block [13]. The precession frequency of the spins during the pulse is, in a frequency modulated frame:

$$\Omega_{\mathrm{eff}} = \sqrt{[\Omega_i - \gamma G_e z - \omega_{\mathrm{rf}}(t)]^2 + \omega_1(t)^2}, \tag{26}$$

where ω_{rf} is the instantaneous frequency of the pulse and ω_1 is the pulse amplitude. This gives, for the spatial derivative of the spin phase at the end of the chirp+gradient block:

$$K(z) = \int_0^{T_e} \frac{d}{dz}\sqrt{[\Omega_0 - \gamma G_e z - \omega_{\mathrm{rf}}(t)]^2 + \omega_1(t)^2}\, dt + \gamma G_e T_e, \tag{27}$$

where the second term on the right-hand side is due to the additional gradient pulse after the chirp pulse. This expression can be used in Eq.3 together with an effective diffusion time $\Delta' = \Delta - T_e$ to simultaneously use an accurate expression for the effective gradient and account for the effect of finite gradient pulses. This was found to give the best agreement between numerical simulation and analytical expressions [17]. Note that while accurate numerical simulation are possible, analytical expressions are useful for the fast processing of experimental data.

2.2. Spatially resolved acquisition

In spatially encoded DOSY, the diffusion information is encoded in the attenuation of the magnetisation as a function of the position in the NMR tube. Fast spectroscopic imaging is needed during acquisition to decode this information for several chemical sites simultaneously. Following Shrot and Frydman, we are using echo-planar spectroscopic imaging (EPSI) [23], which provides a spatial profile for each frequency in a single scan. The EPSI pulse sequence element is shown in Figure 4.a. It consists of a train of bipolar gradient pulses of amplitude $\pm G_a$ and of duration T_a each. This results in a zig-zag trajectory in a two-dimensional (k, t) space, shown in Figure 4.b, with:

$$k(t) = \gamma \int_0^t G_a(t')dt' - \frac{\gamma G_a T_a}{2}. \tag{28}$$

k(t) is the integrated area of the acquisition gradient multiplied by the gyromagnetic ratio, and corresponds to the spatial frequency that is sampled. The spectroscopic imaging data is obtained by 2D Fourier transformation. The so called odd and even echoes, corresponding to data acquired with positive and negative gradients, are often processed separately, so that fast Fourier transformation (FFT) can be used to go from the time to the frequency domain. In the spectral dimension, the spectral width is governed by the time spacing between two consecutive points with the same value of k. This spacing, $2T_a$, results in a spectral width of:

$$SW_{\mathrm{conv}} = \frac{1}{2T_a} \tag{29}$$

The filter bandwidth during acquisition is chosen to be larger than the frequency dispersion induced by the magnetic field gradient ($\gamma G_a L_s$), and is typically of several tens of kilohertz. As a result, the chemical-shift offsets that lie outside the spectral width SW_{conv} are not filtered out and are instead folded, through a translation by an integer multiple of SW_{conv}. Resolution

in the spectral dimension is governed, as in conventional experiments, by the total acquisition time:

$$\delta v = \frac{1}{2T_a N}, \tag{30}$$

where N is the number of loops in the EPSI block.

In the spatial dimension, spatial resolution is governed by the maximum spatial frequency that is sampled, i.e., by the maximum value of the variable k:

$$\delta z = \frac{2\pi}{\gamma G_a T_a} \tag{31}$$

and the field of view is given by:

$$FOV = \frac{2\pi}{\gamma G_a \delta t}, \tag{32}$$

where δt is the delay between two sampled points. The field of view is not a limitation as δt can be chosen to be small enough so that $FOV > L_s$, with no consequences on the other parameters or on sensitivity.

Experimentally, the minimum value that can be used for T_a is limited by the ramp time of the gradients, as well as by instabilities that may occur for fast oscillating gradient waveforms. This sets a limitation on the spectral width that can be achieved. Spectral resolution is limited by the maximum duration which the hardware can sustain during the EPSI block. On the other hand, and in contrast to UF2DNMR experiments such as UFCOSY [24], the maximum acquisition gradient that can be applied is typically not a limitation. DOSY data sets indeed usually have only 8 to 32 points in the incremented dimension, compared to 64 or more points for other 2D experiments.

Obtaining spatial resolution comes with a sensitivity penalty compared to purely spectroscopic acquisition. If, using EPSI, a sample of length *L* is divided into *M* pixels (keeping the same acquisition time), then sensitivity will decrease by a factor *M*. When comparing conventional and SPEN DOSY experiments, the penalty in terms of sensitivity per square root of experiment time due to spatial resolution is then $\sqrt{M}$. In SPEN DOSY experiment, the choice of acquisition gradient is a compromise between the number of points for the diffusion decay curve (higher G_a gives more points) and sensitivity (higher G_a reduces the signal-to-noise ratio). On the other hand, EPSI has in principle no sensitivity penalty compared to a gradient echo acquisition that would achieve the same spatial resolution in the same total acquisition

time but without spectral resolution [25]. In practice, the sensitivity of EPSI is slightly lower if ramp sampling is not used.

Single-scan echo planar spectroscopic imaging data can in principle be processed in pure absorption, provided that the pulse sequence is timed so that chemical shift evolution is refocussed at the centre of the first readout gradient. This is in contrast to UF2DNMR experiments, where pure-absorption processing is not always possible and requires multiple scans. However, in practice, gradient imperfection can result in distortions in the spectrum and often make magnitude processing a more straightforward option.

Because chemical shift offsets are active during the readout gradient pulses of the EPSI block, the resulting 1D images are shifted by a quantity:

$$\Delta z^{CS} = \frac{\Omega_i}{\gamma G_a}. \tag{33}$$

This chemical-shift displacement is accounted for during data processing. Equivalently, this corrects for the shearing of the zig-zag trajectory in (*k*-*t*) space.

2.3. Convection compensation

The measurement of diffusion coefficients by NMR can yield erroneous results when translational molecular motion other than diffusion are also present [26]. This is the case for flowing samples, and in the presence of sample convection. Convection is always present to some extent and is particularly pronounced for low-viscosity solvents and when the sample temperature is far from room temperature [26]. It is caused by temperature gradients in the NMR tube, which cause the hotter part of the solution to rise while the colder part moves in the opposite direction. In diffusion NMR, this usually leads to a loss in sensitivity, faster decay and in some cases oscillatory curves.

There are several solutions to avoid the problems caused by convection. First, one may work in conditions unfavourable for convection to appear, e.g., by using a smaller diameter or a different material for the NMR tube, by increasing the gas regulation flow to homogenize temperature within the sample, by restricting the sample length using Shigemi tubes, or by spinning the sample [26,27]. Second, one may use pulsed-field gradients along a transverse axis to encode diffusion in a direction perpendicular to the convection [28]. However, this requires a triple-axis gradient probe. Further, for SPEN DOSY, the small diameter of the tube is a limitation, and a reference profile is needed for the processing [18].

Another solution to mitigate the effect of convection on diffusion measurements, introduced by Jerschow and Muller [29] for conventional DOSY, is to use two diffusion-encoding steps set up such that the effect of diffusion is cumulative while that of convection cancels out. The convection compensated double-stimulated-echo (DSTE) SPEN DOSY pulse sequence is shown in Figure 2.c [20]. Its mechanism is analogous to that of conventional DSTE DOSY pulse sequences.

Consider a volume element submitted to a pair of diffusion-encoding pulsed-field gradient along z, while moving with a velocity v_z. Compared to the static case, this results in an additional phase of the form, assuming narrow pulsed-field gradients:

$$\phi_v(z) = q^* v_z \Delta \tag{34}$$

where q^* is the area of the diffusion-encoding gradient multiplied by the gyromagnetic ratio and by the coherence order (±1) selected for the dephasing step. The signal attenuation is then:

$$S(q) = \mathrm{S}_0 e^{-\mathrm{D}q^2\Delta} e^{iq^* v_z \Delta}. \tag{35}$$

The acquired signal is a sum over a distribution of values of v_z. It may be oscillatory, and fitting it with the Stejskal-Tanner equation yields erroneous values of the diffusion coefficients. In the double stimulated echo pulse sequence, two diffusion encoding steps are used and the signal attenuation is:

$$S(q) = \mathrm{S}_0 e^{-\mathrm{D}{q_1}^2\Delta/2} e^{iq_1^* v_z \Delta/2} e^{-\mathrm{D}{q_2}^2\Delta/2} e^{iq_2^* v_z \Delta/2}. \tag{36}$$

If the pulse sequence is set such that $q_1^* = -q_2^*$, e.g., by using identical diffusion-encoding pulses and opposite coherence orders for the two diffusion-encoding steps, then a pure diffusion attenuation is retrieved.

In the case of the STE SPEN DOSY pulse sequence, there is similarly an additional dephasing due to velocity

$$S(z) = \mathrm{S}_0 e^{-\mathrm{D}K(z)^2\Delta} e^{\mathrm{i}K^*(z) v_z \Delta} \tag{37}$$

where

$$K^*(z) = pK(z). \tag{38}$$

For the DSTE SPEN DOSY pulse sequence, the attenuation becomes

$$S(z) = \mathrm{S}_0 e^{-\mathrm{D}K_1^*(z)^2\Delta/2} e^{iK_1^*(z) v_z \Delta/2} e^{-\mathrm{D}K_2^*(z)^2\Delta/2} e^{iK_2^*(z) v_z \Delta/2}. \tag{39}$$

Compensation of the velocity induced phase term is obtained for $K_1^*(z) = -K_2^*(z)$ by using identical diffusion-encoding blocks and opposite coherence orders. However, because of the

use of a second stimulated echo, the sensitivity will drop by 50% compared to a classical STE experiment.

3 Experimental

3.1 Hardware

All the experiments were carried out on a Bruker Avance III spectrometer operating at a ^{1}H Larmor frequency of 500.13 MHz, equipped with a 5 mm dual $^{1}H/^{13}C$ cryo-probe with single-axis gradients or a room-temperature 5 mm TXI $^{1}H/^{13}C/^{15}N$ probe with triple-axis gradients. The gradients were calibrated along each axis using a Shigemi tube filled with doped water (1% H_2O+0.1% $CuSO_4$ in D_2O) and a restricted sample length of 10 mm. The temperature inside the probe was calibrated with a standard methanol sample and then set to a value of 298 K with airflow of 535 L/h. All the experiments were done without sample rotation.

3.2 Samples

The solution mixtures were prepared according to the following procedures:

Mixture 1 (M1). 14.8 mg of caffeine were dissolved in a vial in 750 µL of D_2O. The solution was shaken until complete dissolution. In that solution was added 7.2 µL of ethyl acetate, 5.3 µL of DMSO and 3.0 µL of methanol. The concentration of each molecule is about 100 mM. 600 µL of this solution was withdrawn and introduced into a 5 mm NMR tube. A sample was similarly prepared in a 5 mm Shigemi tube restricted to 10 mm for conventional DOSY experiments.

Mixture 2 (M2). To 600 µL of D_2O was added 24.3 µL of methanol, 35.0 µL of ethanol and 44.9 µL of propanol. The concentration is near 1 M for each compound. The sample was well shaken and poured into a 5 mm NMR tube.

Mixture 3 (M3). In a vial, 14.6 mg of caffeine was weighted and then was dissolved in 750 µL of $CDCl_3$. The solution was shaken until complete dissolution. In that solution 7.2 µL of ethyl acetate, 5.3 µL of DMSO and 3.0 µL of methanol was added. The concentration of each molecule was about 100 mM. 600 µL of this solution was withdrawn and introduced into a 5 mm NMR tube.

3.3 Processing

All the experiments were processed using a custom-written MATLAB code, which is available upon request. The process is illustrated in Figure 5. First, the data is read from Bruker format and reshaped into a 2D matrix. Then the data is apodised in the time dimension. For data

processed in pure absorption, a cosine window is used, while for data processed in magnitude, a sine window is used. Apodisation can be done in the k dimension using, e.g., a Hamming window, but this was not used here. Next, zero filling in the time dimension is applied prior to 2D Fourier transform. Here, no zero filling was applied in the k dimension. Peak picking is then performed on a ^{1}H 1D spectrum, to obtain the correct values of the chemical-shift offsets even for peaks that are folded in the EPSI data. Regions are then defined on a slice of the EPSI data to calculate the intensity or area for each peak. Then for each peak, corrections for the chemical shift displacements during encoding and acquisition are performed, and the diffusion curve is plotted and fitted to the modified Stejskal-Tanner equation to estimate the corresponding diffusion coefficient. A DOSY map is generated in the usual way, by placing, for each peak, a peak with a gaussian shape in the diffusion dimension, with its centres given by the estimated diffusion coefficient and its width given by the estimated uncertainty of the fit. The DOSY map is finally displayed as a contour plot. The code used to create the DOSY map was adapted from the DOSY Toolbox / GNAT [30,31].

The conventional DOSY experiment was processed using a custom-written MATLAB code. For the comparison of signal to noise ratio, the data is read from Bruker format and reshaped into a 2D matrix. Then, the data is apodised in the time dimension with a cosine window. Next, zero filling in the time dimension is applied prior to Fourier transform in time dimension. The signal to noise ratio was then calculated on the DMSO peak.

For the complete processing of the conventional data, first, the data is read from Bruker format and reshaped into a 2D matrix. Next, zero filling in the time dimension is applied prior to Fourier transform in time dimension. Peak picking and regions are defined on the spectrum obtained with the lowest diffusion gradient. The diffusion curve is plotted and fitted to the Stejskal-Tanner equation to estimate the corresponding diffusion coefficient. A DOSY map is generated in the usual way, by placing, for each peak, a peak with a gaussian shape in the diffusion dimension, with its centres given by the estimated diffusion coefficient and its width given by the estimated uncertainty of the fit. The DOSY map is finally displayed as a contour plot. The code used to create the DOSY map is the same than for the SPEN DOSY processing.

4 Results and discussion

An example of DOSY map obtained with the SPEN DOSY experiment is shown in Figure 6.b. The data was obtained in a single scan of less than 200 ms, on a sample composed of ethyl

acetate, DMSO, methanol and caffeine in D_2O (sample M1). It will be used to illustrate the choice of encoding and acquisition parameters. The corresponding 1D spectrum can be seen in Figure 6.a, with an assignment of the signals that will be used in following figures. The result of a conventional DOSY experiment on the same sample is shown in Figure S1, and the resulting estimated diffusion coefficients are shown in Table S1. There are systematic differences between the two, which may originate from the different influence of gradient non uniformity in conventional and SPEN experiments and is outside the scope of the present work.

4.1 Spatial region

The first decision to make when setting up the SPEN DOSY experiment is the length of the region swept by the chirp pulse. It should correspond to a region where the coil's sensitivity and the magnetic-field gradient are sufficiently homogeneous. For ^{1}H experiments, a length of 15 mm and 20 mm can typically be used on indirect-detection and direct-detection single-axis-gradient probes respectively. On triple-axis gradient probes, the magnetic field gradient along the longitudinal axis has poor uniformity (the field gradient is steeper at the centre of the coil). If this is not taken into account during processing, a length of up to 10 mm can be used as a compromise between sensitivity and the effect of gradient non-uniformity. These lengths were determined on commercial probes manufactured by Bruker and may need to be adjusted for other probes.

Smoothed chirp pulses are typically used for spatial encoding in SPEN DOSY experiments. The actual shape of the B_1 amplitude is not very important. Here we use pulses with a plateau for the central 80% of the shape, and a smooth transition between 0 and B_{1max} on the edges. As a result, only the central 80% of the swept region is used for data fitting. This can be extended by correcting the data by the selection profile of the chirp pulse.

4.2 Spatial encoding parameters

For a given length L_S of the swept region, the maximum attenuation of the diffusion decay curve is determined by the diffusion delay (Δ), and by the product of the duration of the swept pulse, T_e, and the intensity of the encoding gradient, G_e (or, equivalently for a fixed L_S, the product of the duration of the swept pulse, T_e, and its bandwidth, BW). This product plays a role analogous to the area of the diffusion-encoding pulsed-field gradients in conventional DOSY. These values should be set, as in conventional DOSY, so that the maximum attenuation is sufficient while still achieving sufficient sensitivity. A compromise is usually needed when

there is a range of diffusion coefficient values in the sample. For the data shown in Figure 6.b, the parameters are a chirp of duration (T_e) 1.5 ms sweeping over 110 kHz (BW) applied with an encoding gradient (G_e) of 25.9 G/cm (35.7 % of the maximum gradient intensity) and diffusion delay equal to 100 ms.

Figure 7.a shows the results of a series of SPEN STE DOSY experiments in which the duration and the bandwidth of the chirp pulses were changed, while keeping the product of the two, as well as the length of the swept region, constant. These parameters are displayed in Table 1. The estimated diffusion coefficients agree for all the experiments within the uncertainty estimated from the fit. Note that the larger uncertainty for methanol and HOD diffusion coefficients comes from the fact that the maximum gradient area was chosen to favour the measurement of lower diffusion coefficient. The choice of specific values of T_e and BW is governed by the RF limitation of the probe. For a given time-bandwidth product, the shorter the pulse, the higher the maximum B_1 amplitude required to achieve an adiabatic 180° rotation. The signal-to-noise ratio, measured on the DMSO peak, was also compared for the choices of parameters given in Table 1. For a given time-bandwidth product, the specific choice of duration and bandwidth of the pulse has virtually no influence on SNR as shown on Figure 8.a.

Figure 7.b shows the results of a series of SPEN STE DOSY experiments on M1 in which the duration of the chirp pulses was changed, for a given bandwidth with the parameters shown in Table 2. It can be seen that the uncertainty of the fit tends to first decrease when the time-bandwidth product of the encoding pulse increases. It can be seen from the HDO peak that strong attenuation increases further the uncertainty.

4.3 Acquisition parameters

The acquisition parameters are chosen according to the relationships given in section 2.2. For sample M1 (Figure 6.b), a value of Ta = 307 µs was used, which results in a spectral width of 1630 Hz, and a train of 240 bipolar pulses was used, which results in an acquisition time of 147 ms.

A series of experiments were carried out to illustrate the effect of two parameters of the EPSI acquisition, the intensity of the readout gradients and the duration of the acquisition (i.e., the number of loops of the EPSI acquisition). The data can be processed in pure-absorption and in magnitude mode, and the two are compared here. The comparison between two is shown in figure 9 for the same dataset. The diffusion constants obtained from

these two processing modes are comparable, however, and improvement in spectral resolution is achieved with pure-absorption processing.

For a given duration of the readout gradient, the resolution of the image is determined by the intensity of the gradient. Figure 10.a shows the result of a series of SPEN STE DOSY experiments acquired with increasing readout gradients on the same mixture as previously (M1). For each experiment, the diffusion coefficient calculated for each signal and the uncertainty of the fit were extracted and compared, for both pure-absorption and magnitude processing. For low values of the readout gradient, the uncertainty of the fit becomes very large, and in this case values of about 20 G/cm or more should be used. For larger intensities of the readout gradients, the results are consistent irrespective of G_a for magnitude mode processing. For pure-absorption processing, there is more variability as a function of G_a, and a systematic deviation is also observed for the caffeine peaks.

Increasing the intensity of the readout gradient also influences the signal to noise ratio for the experiment. The signal to noise ratio of the DMSO peak was calculated as a function of the readout gradient intensity for each experiment, and the results are shown in Figure 8.c. As expected, the signal to noise ratio decreases when gradient increases. A choice has to be made between signal to noise ratio and number of points for the fit. As shown previously, the acquisition gradient also has an impact on the resolution hence the number of points of the fit as shown with the second axis on Figure 10.a and Figure 8.c. It can be noted that in each case the SNR is better with pure-absorption processing by a factor around $\sqrt{2}$.

Despite increased resolution and sensitivity, pure-absorption processing results here in lower-quality estimates of the diffusion coefficients, because of distortions in the spectrum induced by the strong and oscillating acquisition gradients. Improved phase correction methods, which correct for phase errors that depend on the gradient amplitude, are under development and will be needed for a reliable use of pure-absorption processing.

The second parameter that was investigated was the acquisition duration. A series of experiments were acquired with an increasing number of loops for the EPSI on the same model sample (M1). The diffusion coefficients were extracted and are compared in Figure 10.b. as a function of the acquisition duration. For this relatively sparse spectrum, for most of the peaks, the results are similar irrespective of the acquisition duration. Only the methanol and one of the caffeine peaks show significant changes when the acquisition is too short. This is due to the loss of resolution when the acquisition duration is reduced. As the peaks are close

to each other, poor spectral resolution yields meaningless fitting curves and diffusion coefficients values.

The effect of the acquisition duration on the signal to noise ratio was also investigated. The signal to noise ratio of the DMSO peak was calculated and plotted in Figure 8.d for each experiment. In this regime where the acquisition duration remains smaller than the transverse relaxation time, the longer the acquisition is the higher the signal to noise ratio becomes, as in conventional experiments. However, the acquisition duration is limited here by the duty cycle of the gradient unit and gradient instabilities.

4.4 Coherence selection gradient

Single-scan acquisition also requires that pulsed-field gradients are used to select the required coherence transfer pathway. CTP selection gradients are shown on two separate lines in Figure 2. When multiple gradient axes are available, it is preferable to achieve spatial encoding and CTP selection with different axes, to avoid interference between the two.

In the SPEN STE DOSY pulse sequence, a spoiler gradient is applied between the second and third 90° pulses (f), to destroy the transverse magnetisation. Pairs of gradient pulses are used around the chirp pulses (a and b), to select only magnetisation that is refocused. When triple-axis gradients are available, a further pair of gradient pulses (c) is used to select the anti-echo pathway even for slices that have a null net area of the diffusion-encoding gradient. This gives some flexibility in the choice of the duration of the post-chirp gradient.

Figure 11 shows the effect of a modification in the CTP selection gradients, when they are applied along the same axis as the diffusion-encoding gradients (in this case using a single-axis gradient probe). Several SPEN DOSY experiments were done on a mixture of alcohols (M2) in order to illustrate this effect. Experiment 1 is taken as a reference, with $a \neq 0$, $b \neq 0$ and $c = 0$. Gradients a and b are respectively increased by 16 G/cm in experiment 2 and in experiment 3, and c is non-zero in experiment 4 and 5. This comparison shows that the gradient pulses a and b have only limited effect on the estimated diffusion coefficient, while gradient c shows a significant effect and hence should not be used on a single-axis-gradient probe if the fitting function is not modified to take c into account.

Further gradient pulses ($g1 = -f$, $g2 = -2a + c$, $g3 = -2b + c$) are included in the pulse sequence to compensate for the CTP gradients, as this is expected to reduce the effect of diffusion-encoding and CTP-selection gradients on the acquired signal.

Note that for the DSTE SPEN DOSY experiment, no combination of CTP-selection gradient was found to implement the pulse sequence with a single gradient axis.

4.5 Sensitivity

While spatial parallelisation makes it possible to acquire 2D experiments in a single scan, this acceleration comes at a price in sensitivity. A comparison of signal-to-noise ratio was done here between conventional and SPEN DOSY on sample M1. The conventional DOSY was carried out with 16 gradient increments and 8 scans per increment. To obtain comparable results with SPEN DOSY, the acquisition gradient was chosen to sample an 8 mm region with 16 points, and 128 scans were added to have the same total experiment duration. The other parameters were the same (recovery time, gain…). The acquisition time for the conventional DOSY was intentionally set to the short value (147 ms) to which SPEN DOSY is limited, to focus on the effect of spatial parallelisation, and the data were processed identically. The results are compared in Table 3, for each peak in the spectrum. The conventional experiment is more sensitive by a factor ranging from ~3 to ~7. In theory one expects a penalty for the SPEN experiments of about 7: i/ a sensitivity penalty due to the spatially resolved acquisition, which is 16 when 16 pixels are resolved; ii/ a sensitivity advantage of 4 because 128 scans are averaged in the SPEN experiment, vs 8 scans in the conventional experiment iii/ a further penalty of $\sqrt{2}$ because only odd echoes are processed; iv/ a penalty of 1.25 because only the central 8 mm of the sample are used in SPEN DOSY. While the agreement between the theoretical and experimental loss is only qualitative, as it does not account for additional contributions such as offsets, relaxation rates, etc, it provides a useful guide to assess the feasibility of SPEN DOSY experiments.

When the spectrum is sufficiently sparse, a spatial profile can be obtained for each peak by applying a weak and continuous gradient during acquisition. For the SPEN DOSY experiment, a similar encoding scheme turns the peaks into diffusion curves from which it is possible to extract diffusion coefficient. A sensitivity comparison was made between the two methods. The encoding step, acquisition time, and maximum value of *k* were kept the same for both experiments (the total gradient area in the second acquisition is the same as in the first lobe of the EPSI acquisition). This comparison was performed with a doped water sample. The acquisition done with EPSI give SNR_{EPSI} = 3262 while the acquisition done with the single gradient lead to SNR_{1D} = 7575 hence a factor a 2.32 in favour of the 1D acquisition. The fact

that only odd echoes are processed in the EPSI case accounts for a factor of $\sqrt{2}$. The remaining might be due to gradient imperfections as well as diffusion attenuation during acquisition. The difference is less dramatic than might be expected for moving from a 1D to a single-scan 2D acquisition. However, the large acquisition bandwidth of EPSI does not yield lower sensitivity than a purely spatially resolved acquisition of the same duration that achieves the same spatial resolution [25].

4.6 Convection compensation

Sample convection is a common problem in diffusion NMR experiments. As described in section 2.3. , a solution to this problem is to use a double stimulated echo, which cancels the velocity-induced dephasing. Figure 12 shows the using a double stimulated echo pulse sequence to record SPEN DOSY data in the presence of significant sample convection. The solvent for this sample is deuterated chloroform (sample M3), and the experiment is carried out at a temperature of 313K. While convection results in faster decay and oscillations in the case of the STE experiment, the experiment recorded with DSTE shows good quality data and hence, allows a precise measurement of the diffusion coefficient. However, the cost of convection compensation in this case is a loss in signal to noise ratio by a factor of 2 compared to single STE. Convection compensation is not always needed, however, and in this case mixture 1 and 2 were analysed with a single stimulated pulse sequence.

5 Summary of guidelines

The results described and discussed above make it possible to formulate a set of recommendations for the implementation of the SPEN DOSY experiments for the analysis of mixtures:

- Choose the spectral width in the conventional dimension, through the choice of the duration of the readout gradient (T_a). Values shorter than 200 μs are difficult to achieve for standard hardware. The addition of a spectrally selective pulse can be useful if peaks outside the selected spectral width fold onto peaks of interest.
- Choose the duration of the acquisition block. On usual probes, this is limited by the properties of the gradient coil and amplifier. We use values of ~150 ms on a variety of Bruker high-resolution probes and gradient amplifiers, together with a recycle delay of 5 s or more

- Choose the length of the encoded region, L_S. We use 10 mm on triple-axis gradient probes and 15 mm on single-axis gradient probe.
- Choose the intensity of the acquisition gradient, such that the number of pixels is larger than 30.
- Optimise empirically the product $T_e \times G_e$. This is done in a similar way as for conventional DOSY experiment. Ideally, the maximum attenuation should be by about 80–90%. In practice, when dealing with mixtures, this cannot be achieved for all the molecules at the same time. The uncertainty for the estimate of the diffusion coefficients, and the separation power of the experiment, will be higher for the range of diffusion coefficients that have a maximum attenuation that is neither too small not too large.
- At processing stage, pure-absorption processing can be attempted, and can help to separate compounds in crowded spectra[18]. Depending on the gradient system, however, the phase errors across the data may be large, and one may have to revert to magnitude processing

6 Conclusions

The principles and implementation of spatially encoded diffusion-ordered NMR spectroscopy (SPEN DOSY) have been described and illustrated on a mixture of small molecules. Spatial encoding makes it possible to collect DOSY data in less than one second, and requires specific setup and processing steps. The relationships that govern the choice of encoding and acquisition parameters have been described and demonstrated experimentally, together with their influence on sensitivity. This study should be useful for future applications of SPEN DOSY, that include hyperpolarised and out-of-equilibrium systems.

Acknowledgments

This work has received funding from the European Research Council (ERC) under the European Union's Horizon 2020 research and innovation program (grant agreement no 801774), the Region Pays de la Loire (Connect Talent), the Region Ile-de-France (DIM Analytica) and the Agence Nationale de la Recherche (ANR-16-CE29-0012).

Supplementary material

Comparison between conventional and SPEN DOSY on mixture M1; pulse sequence code for the SPEN DOSY experiments.

References

[1] Bernstein, M. A. *Magn. Reson. Chem.* **2016**, *54* (6), 422.
[2] Wishart, D. S. *J. Magn. Reson.* **2019**, *306*, 155.
[3] Johnson, C. S. *Prog. Nucl. Magn. Reson. Spectrosc.* **1999**, *34* (3–4), 203.
[4] Barjat, H.; Morris, G. A.; Smart, S.; Swanson, A. G.; Williams, S. C. R. *J. Magn. Reson. B* **1995**, *108*, 170.
[5] Pagès, G.; Gilard, V.; Martino, R.; Malet-Martino, M. *The Analyst* **2017**, *142* (20), 3771.
[6] Stejskal, E. O.; Tanner, J. E. *J. Chem. Phys.* **1965**, *42* (1), 288.
[7] Pelta, M. D.; Morris, G. A.; Stchedroff, M. J.; Hammond, S. J. *Magn. Reson. Chem.* **2002**, *40* (13), S147.
[8] Urbańczyk, M.; Koźmiński, W.; Kazimierczuk, K. *Angew. Chem.* **2014**, *126* (25), 6582.
[9] Pudakalakatti, S. M.; Chandra, K.; Thirupathi, R.; Atreya, H. S. *Chem. - Eur. J.* **2014**, *20* (48), 15719.
[10] Frydman, L.; Scherf, T.; Lupulescu, A. *Proc. Natl. Acad. Sci.* **2002**, *99* (25), 15858.
[11] Dumez, J.-N. *Prog. Nucl. Magn. Reson. Spectrosc.* **2018**, *109*, 101.
[12] Loening, N. M.; Keeler, J.; Morris, G. A. *J. Magn. Reson.* **2001**, *153* (1), 103.
[13] Thrippleton, M. J.; Loening, N. M.; Keeler, J. *Magn. Reson. Chem.* **2003**, *41*, 441.
[14] Ahola, S.; Zhivonitko, V. V.; Mankinen, O.; Zhang, G.; Kantola, A. M.; Chen, H.-Y.; Hilty, C.; Koptyug, I. V.; Telkki, V.-V. *Nat. Commun.* **2015**, *6* (1), 8363.
[15] Telkki, V.-V.; Zhivonitko, V. V. In *Annual Reports on NMR Spectroscopy*; Elsevier, **2019**; Vol. 97, pp 83–119.
[16] Ahola, S.; Mankinen, O.; Telkki, V.-V. *Magn. Reson. Chem.* **2017**, *55* (4), 341.
[17] Guduff, L.; Kuprov, I.; van Heijenoort, C.; Dumez, J.-N. *Chem. Commun.* **2017**, *53* (4), 701.
[18] Guduff, L.; Berthault, P.; van Heijenoort, C.; Dumez, J.; Huber, G. *ChemPhysChem* **2019**, *20* (3), 392.
[19] Guduff, L.; Kurzbach, D.; van Heijenoort, C.; Abergel, D.; Dumez, J.-N. *Chem. - Eur. J.* **2017**, *23* (66), 16722.
[20] Hamdoun, G.; Guduff, L.; van Heijenoort, C.; Bour, C.; Gandon, V.; Dumez, J.-N. *The Analyst* **2018**, *143* (14), 3458.
[21] Shrot, Y.; Frydman, L. *J. Magn. Reson.* **2008**, *195* (2), 226.
[22] Valette, J.; Lethimonnier, F.; Lebon, V. *J. Magn. Reson.* **2010**, *205* (2), 255.
[23] Mansfield, P. *Magn. Reson. Med.* **1984**, *1* (3), 370.
[24] Tal, A.; Frydman, L. *Prog. Nucl. Magn. Reson. Spectrosc.* **2010**, *57* (3), 241.
[25] Posse, S.; Otazo, R.; Dager, S. R.; Alger, J. *J. Magn. Reson. Imaging* **2013**, *37* (6), 1301.
[26] Swan, I.; Reid, M.; Howe, P. W. A.; Connell, M. A.; Nilsson, M.; Moore, M. A.; Morris, G. A. *J. Magn. Reson.* **2015**, *252*, 120.
[27] Esturau, N.; Sánchez-Ferrando, F.; Gavin, J. A.; Roumestand, C.; Delsuc, M.-A.; Parella, T. *J. Magn. Reson.* **2001**, *153* (1), 48.
[28] Kiraly, P.; Swan, I.; Nilsson, M.; Morris, G. A. *J. Magn. Reson.* **2016**, *270*, 24.
[29] Jerschow, A.; Müller, N. *J. Magn. Reson.* **1997**, *125* (2), 372.
[30] Nilsson, M. *J. Magn. Reson.* **2009**, *200* (2), 296.
[31] Castañar, L.; Poggetto, G. D.; Colbourne, A. A.; Morris, G. A.; Nilsson, M. *Magn. Reson. Chem.* **2018**, *56* (6), 546.

Abreviations

BW: Bandwidth

CTP: Coherence Transfer Pathway

DOSY: Diffusion ordered spectroscopy

DSTE: Double stimulated echo

EPSI: Echo planar spectroscopic imaging

FOV: Field of view

FFT: Fast Fourier transform

GNAT: General NMR analysis Toolbox

SNR: Signal to noise ratio

SPEN: Spatially encoded

STE: Stimulated echo

SW: Spectral width

Figures

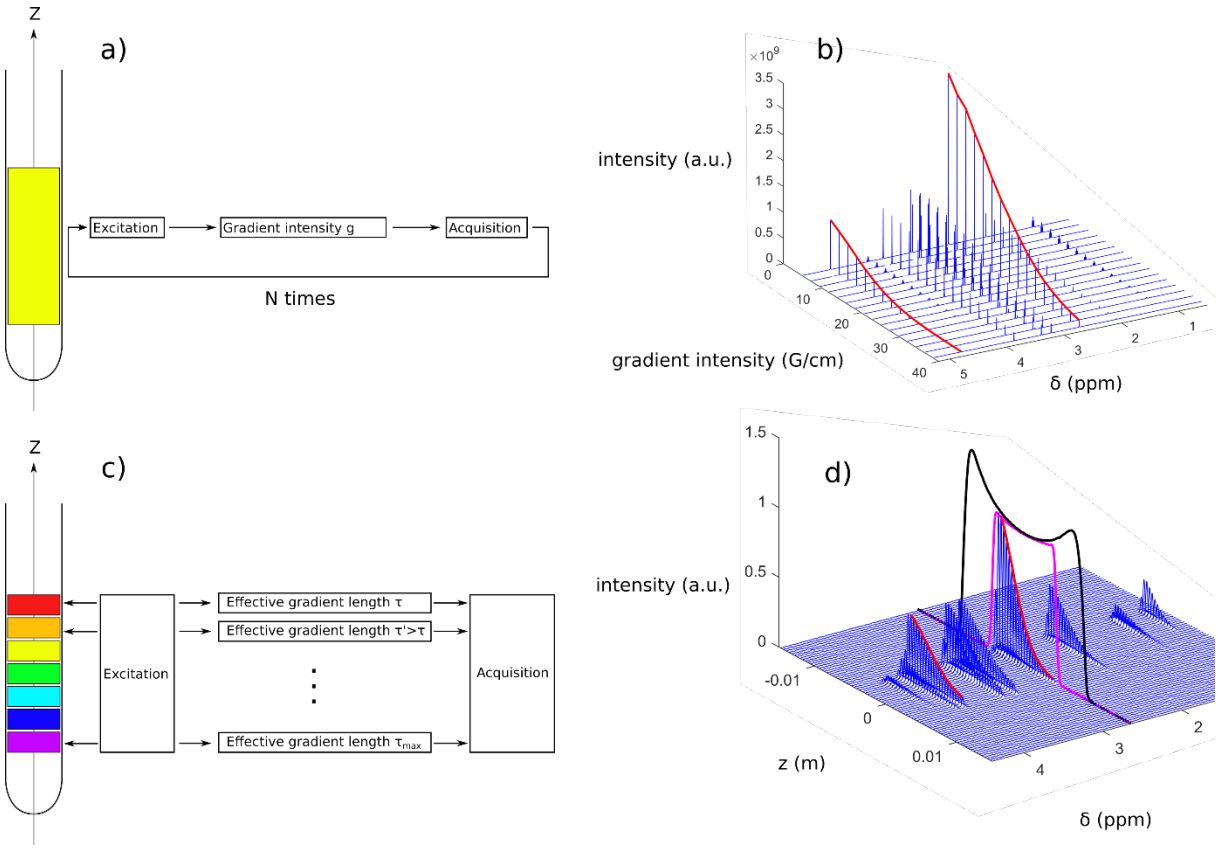

Figure 1: Comparison of the conventional and SPEN DOSY experiments. In conventional DOSY (a), the sub-experiments, corresponding to varying gradient areas, are obtained consecutively. In SPEN DOSY (c), all the sub-experiments are obtained simultaneously. Example data are shown in (b) for conventional DOSY and in (d) for SPEN DOSY. The red lines correspond to the data used for the fit and the calculation of diffusion coefficients. The black line corresponds to a 1D MR image of an NMR tube. The distorted shape of the image comes from the gradient non uniformity. On the edges of the sample, the gradient intensity is smaller than in the centre, leading to a more intense dispersion in the centre than on the edges. The pink line corresponds to a 1D MR image of an NMR tube after the application of a pair of spatially selective 180° chirp pulses.

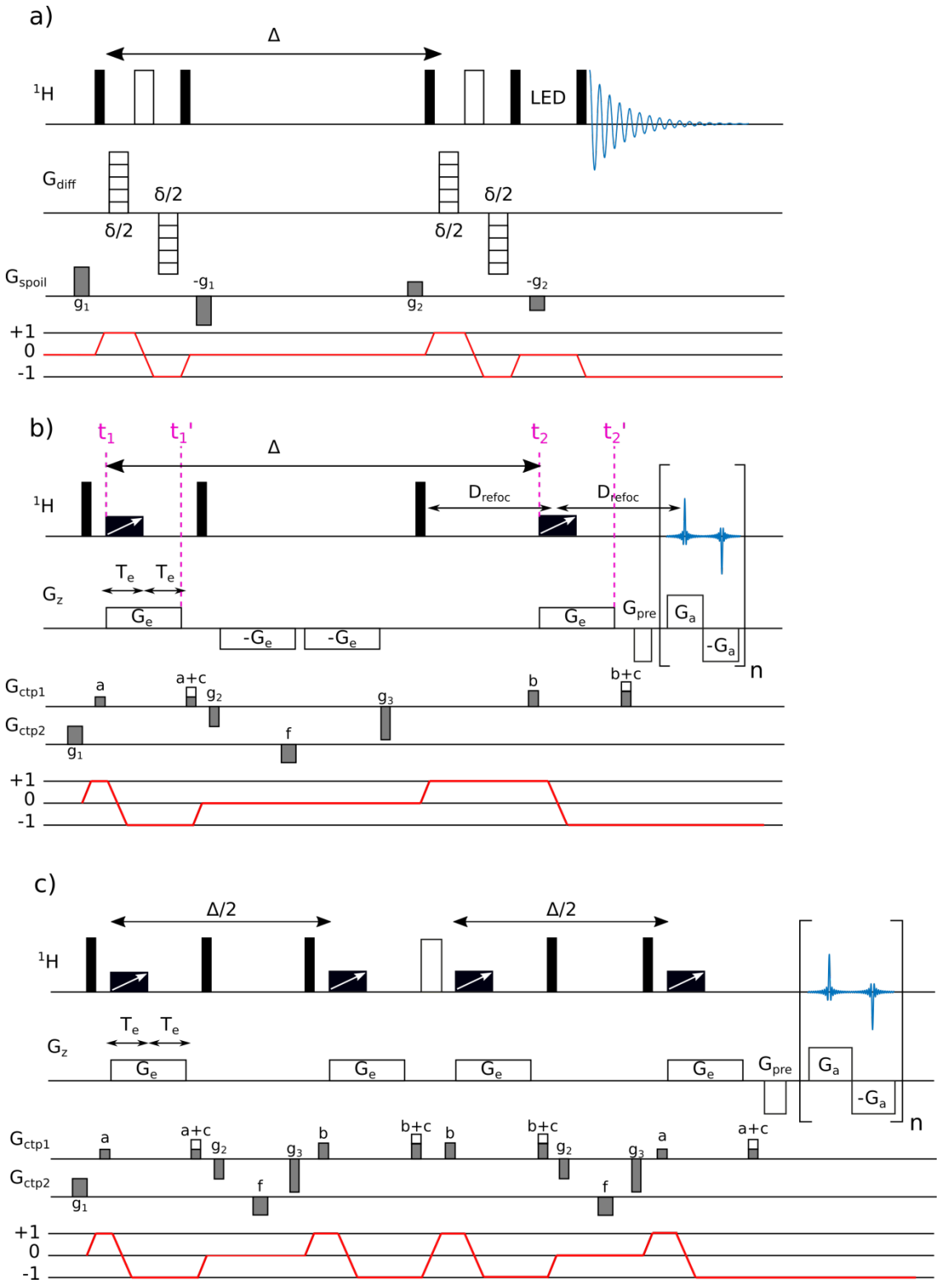

Figure 2: Pulse sequences for conventional and SPEN DOSY experiments. (a) conventional STE DOSY with bipolar gradient pulses (b) SPEN STE DOSY, (c) SPEN DSTE DOSY. Black rectangles correspond to 90° hard pulses, white filled rectangles correspond to 180° hard pulse. Black rectangles with white arrow correspond to frequency sweeping chirp pulse. Out of simplicity, encoding gradient and CTP gradients are displayed on different lines. Red lines correspond to coherence pathways. The start and end times of the spatial encoding block are shown in purple.

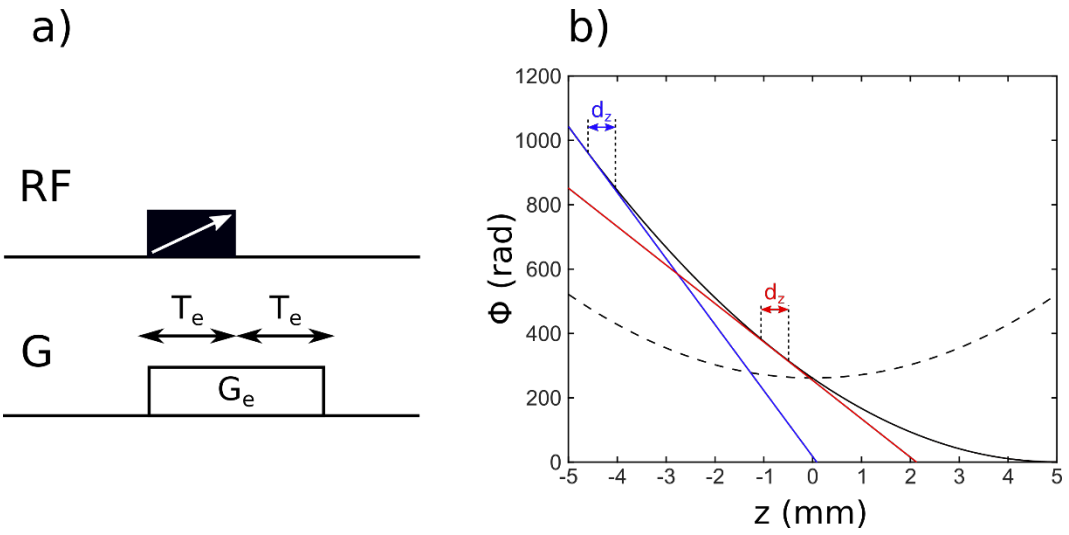

Figure 3: (a) pulse sequence element for spatial encoding of diffusion. (b) Spins' phase variation after the combined application of a magnetic-field gradient pulse and a 180° chirp pulse to an initially transverse magnetisation. The dashed line corresponds to the spins' phase variation just after the chirp pulse. The solid line corresponds to the phase variation after the application of an additional magnetic-field gradient pulse of equal duration. In this example, T_e = 1.5 ms, G_e =26 G/cm and BW = 111 kHz. The derivative of the phase, which correspond to the effective gradient area, is shown for two values of z (in red and blue), showing how diffusion attenuation is position dependent.

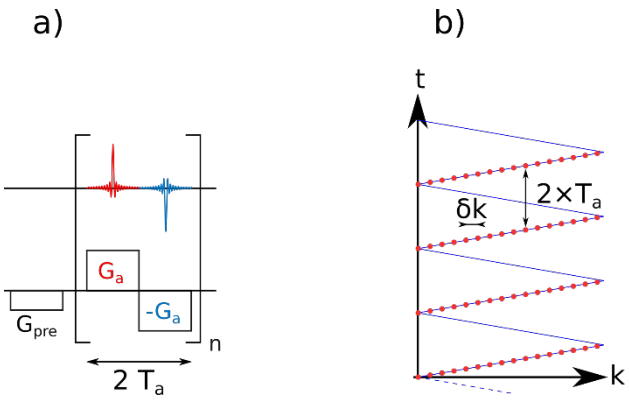

Figure 4: (a) Pulse sequence element for EPSI. (b), resulting trajectory in k-t space...

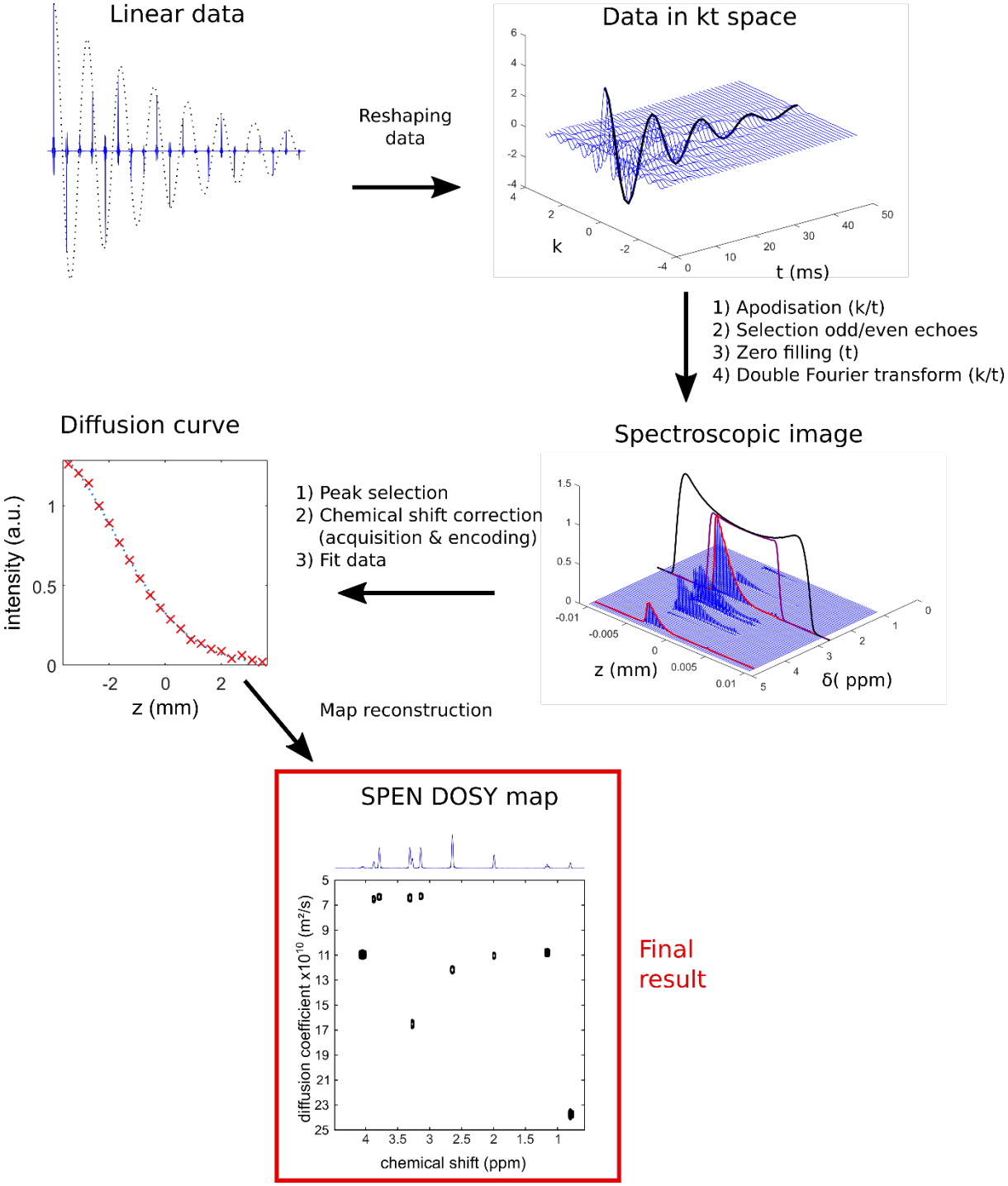

Figure 5: Principle of the SPEN DOSY processing

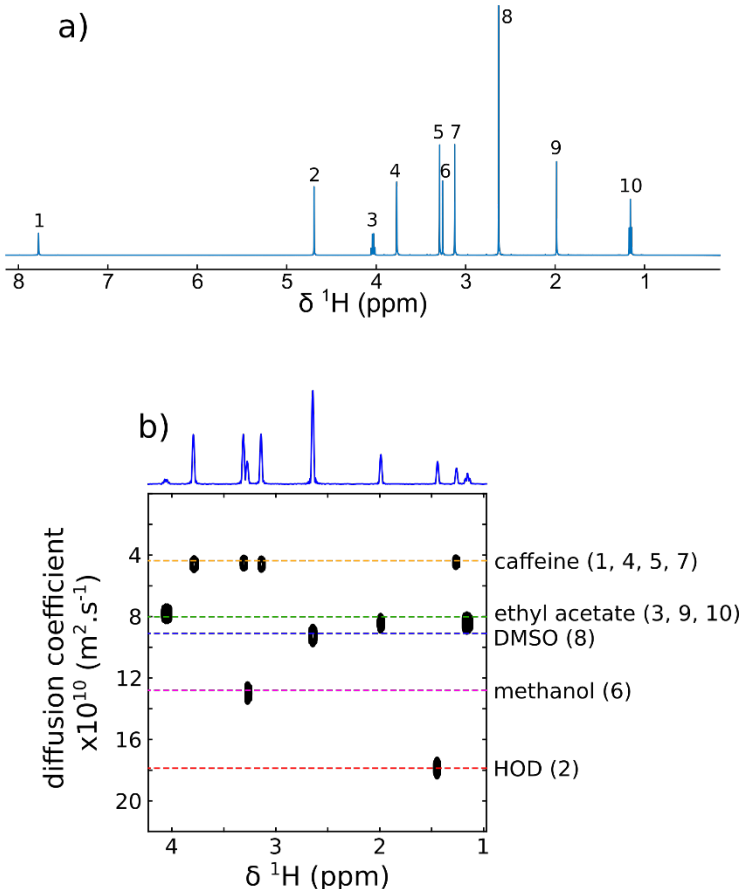

Figure 6:(a)1D ^{1}H spectrum of model mixture 1 and assignments of signal for the evaluation of the effects of parameters. Signals 1, 4, 5 and 7 correspond to caffeine, signal 2 corresponds to HOD, signals 3, 9 and 10 correspond to ethyl acetate, signal 6 corresponds to methanol and signal 8 corresponds to DMSO.(b) Example of a SPEN DOSY map obtained with an acquisition of 147 ms on the same mixture (M1).

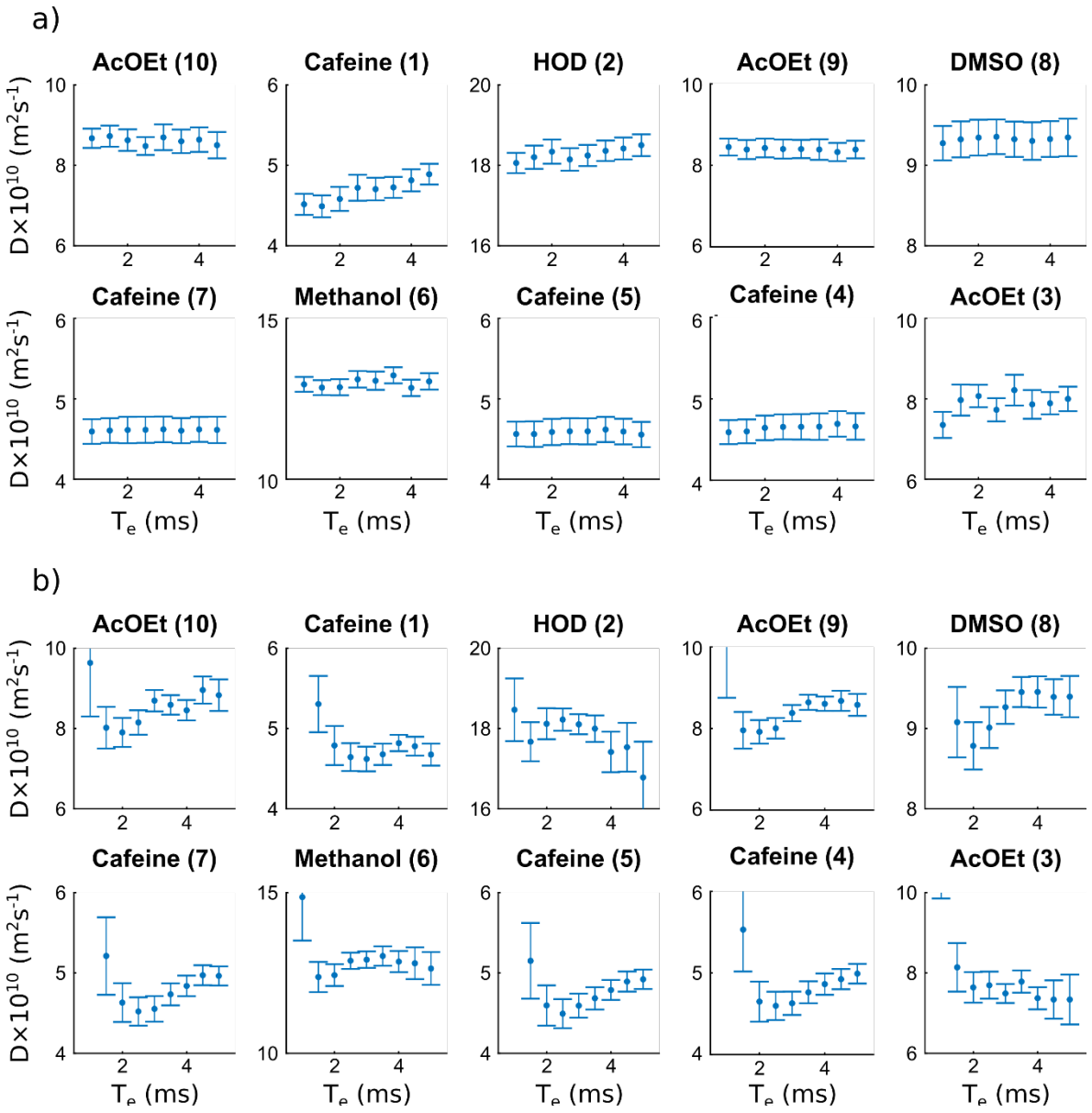

Figure 7: Diffusion coefficient estimated from SPEN DOSY experiments, for each peak of mixture M1, as a function of (a) the chirp duration T_e while keeping the product T_e×BW constant, (b) the chirp duration T_e while keeping BW constant. Error bars correspond to the standard deviation of the fit of the modified Stejskal-Tanner equation. The data is processed in magnitude. The numbers in parenthesis correspond to the signal assignment shown on Figure 6.

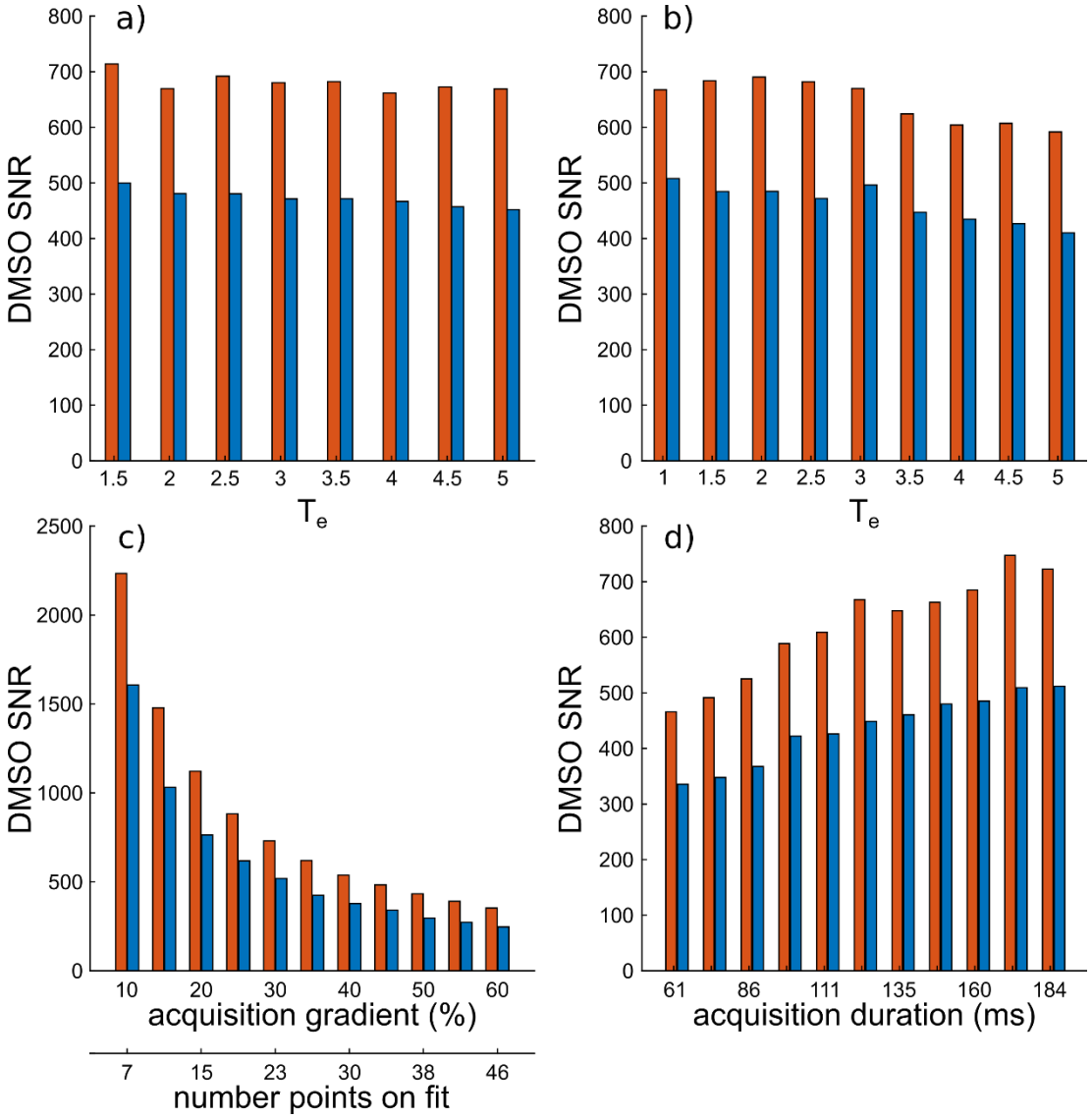

Figure 8: Signal to noise ratio of the DMSO peak in a SPEN DOSY experiment on mixture M1 measured as a function of : the chirp duration while keeping the product T_e × BW constant (a), the chirp duration while keeping BW = 55 kHz (b), the acquisition gradient (c) and the acquisition duration (d). Red bars correspond to pure-absorption data and blue bars correspond to magnitude data.

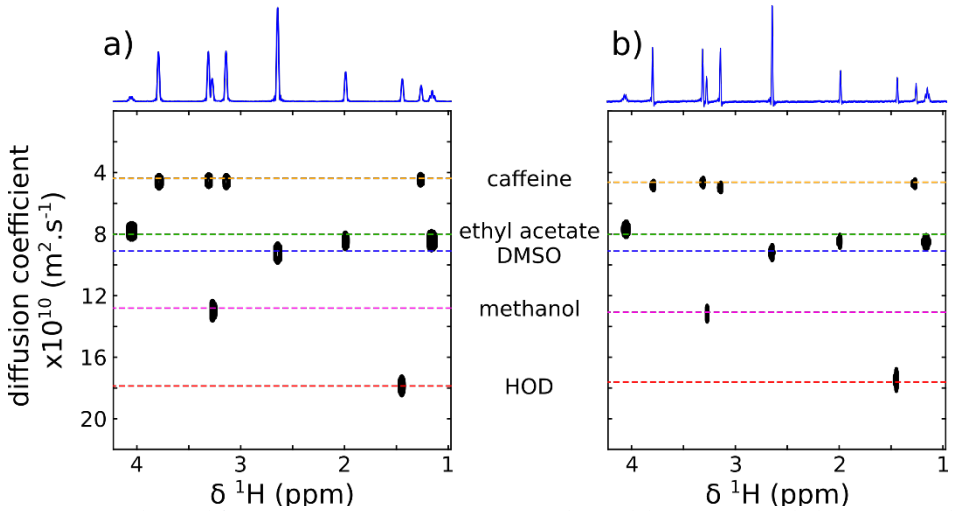

Figure 9: DOSY 2D map obtained from a SPEN DOSY experiment on the model mixture 3, with data processed in magnitude (a) and absorption (b) mode. The 1D spectrum above is a slice extracted from the 2D data before DOSY processing.

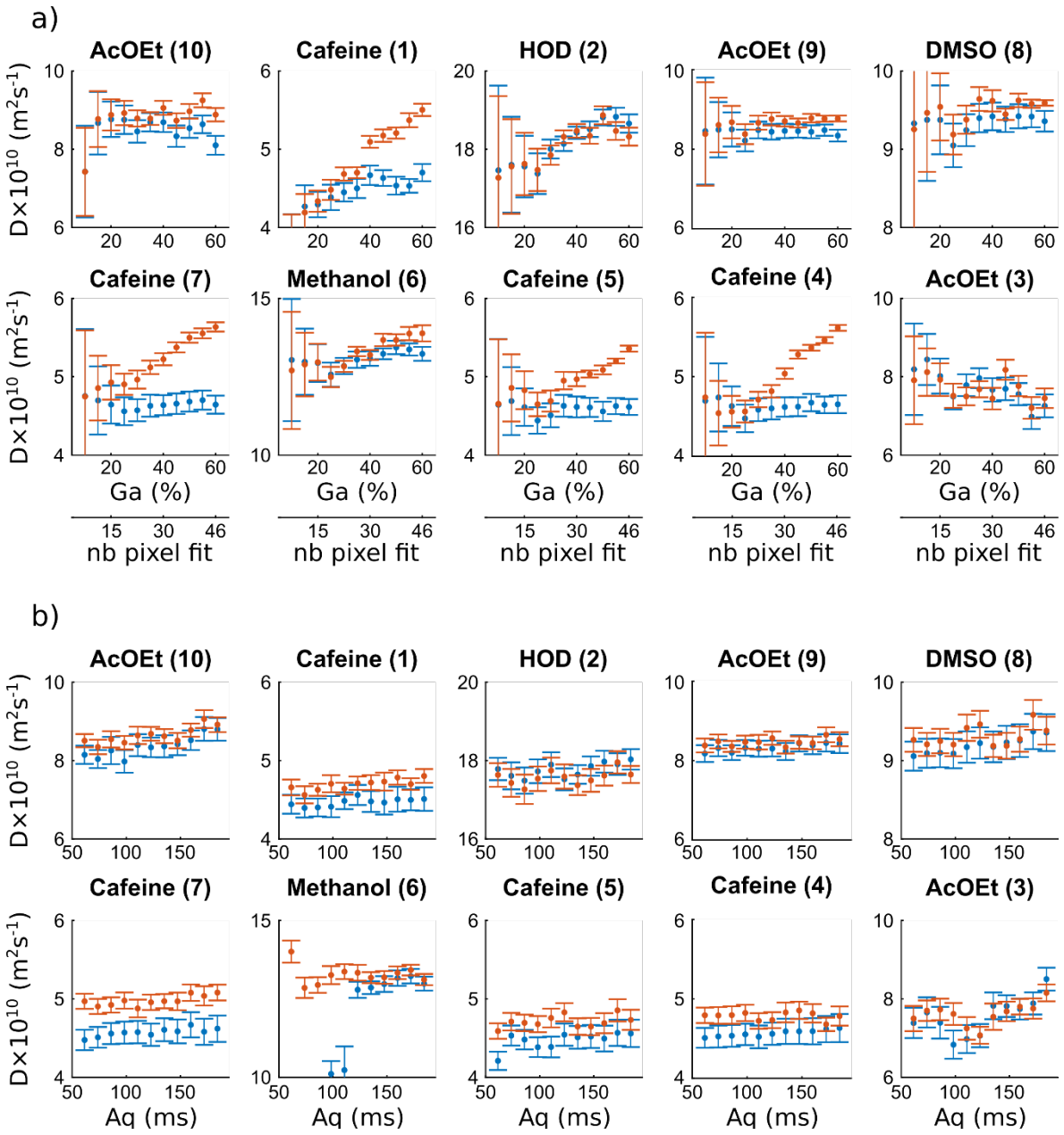

Figure 10: Diffusion coefficient estimated from SPEN DOSY experiments for each peak of mixture M1, as a function of (a) the acquisition gradient, (b) the acquisition duration. The data is processed in magnitude (blue) and pure-absorption (red). The numbers in parenthesis correspond to the signal assignment shown on Figure. 8.

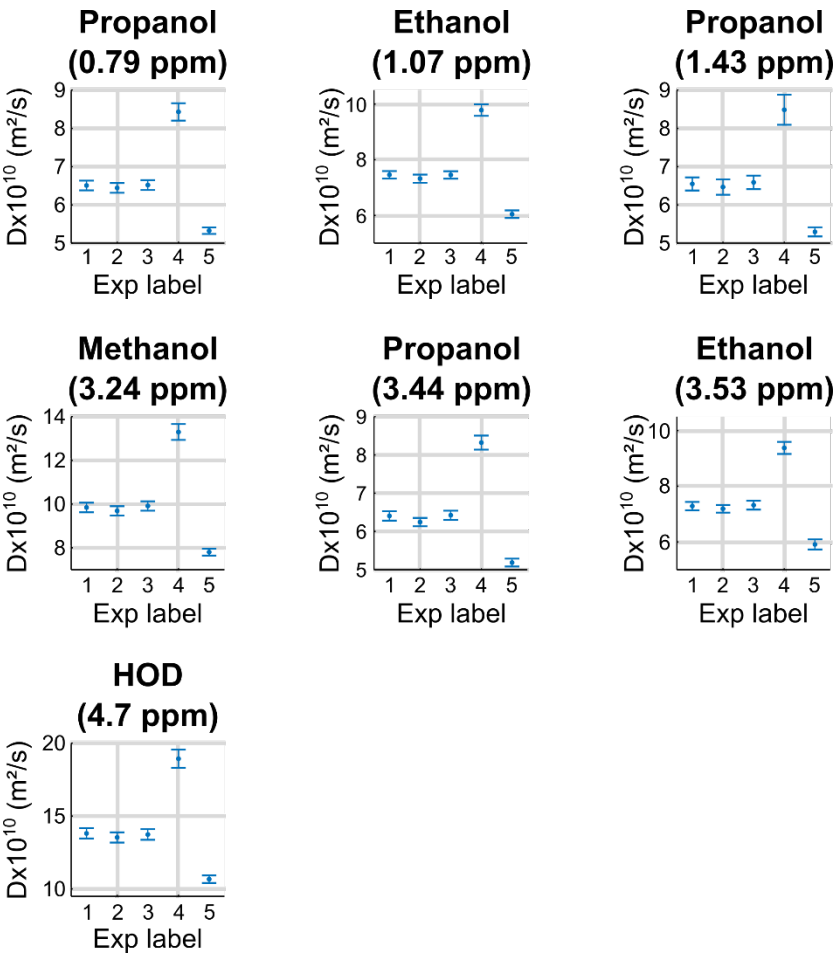

Figure 11: Influence of the CTP gradient on the measurement of diffusion coefficient on a single gradient axis probe. For each signal the diffusion coefficient was calculated in 5 conditions: reference conditions (label 1), with gradient a (see Figure 2). Experiment 1 is taken as a reference, with a ≠ 0, b ≠ 0 and c = 0. Gradients a and b are respectively increased by 16 G/cm in experiment 2 and in experiment 3, and c is non-zero in experiment 4 and 5.

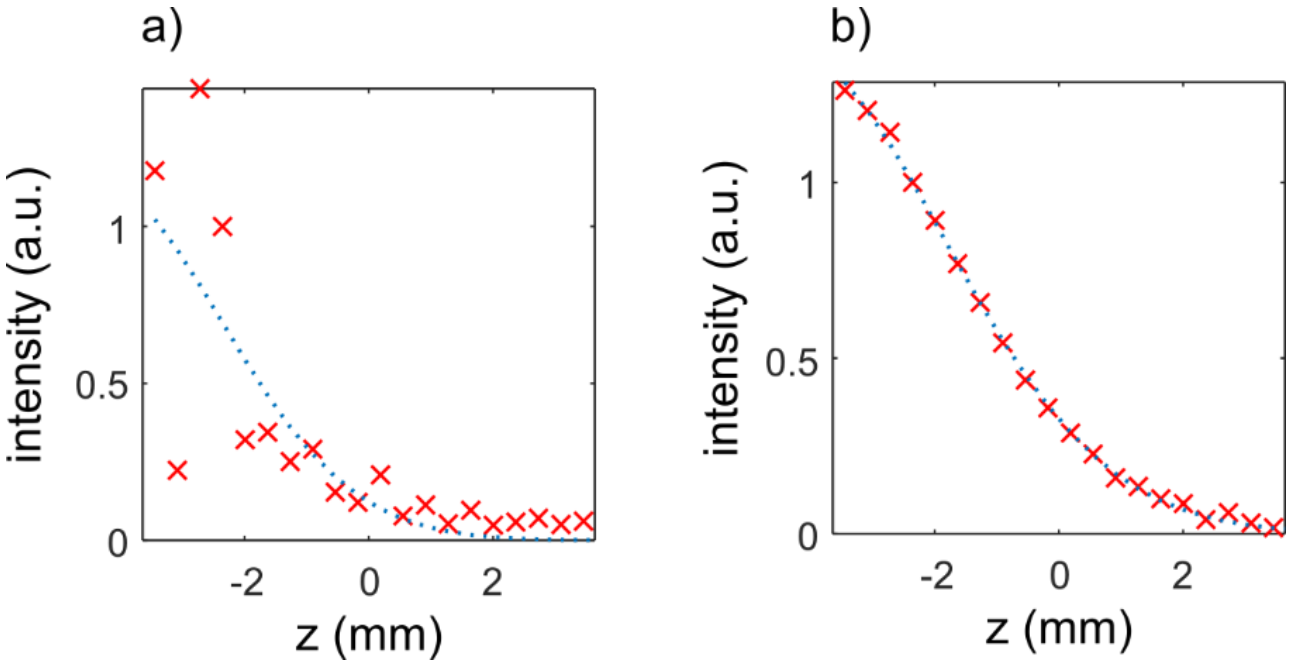

Figure 12: Diffusion decay curves for the DMSO signal, obtained with a SPEN DOSY experiment, on mixture M3, at a temperature of 313 K. In (a) a single stimulated echo is used. In (b), a double stimulated echo is used. The red crosses correspond to the experimental points and the dotted blue lines correspond to the best-fit curve.

Tables

Table 1: Duration and bandwidth of the chirp pulses used in a series of SPEN DOSY experiments to characterise the effect of the time-bandwidth product while keeping it constant

Exp label	T_e (ms)	BW (kHz)	G_e (G/cm)
1	1.5	110	25.9
2	2.0	83	19.6
3	2,5	66	15.5
4	3.0	55	13.0
5	3,5	47	11.1
6	4.0	41	9.6
7	4,5	37	8.7
8	5.0	33	7.8

Table 2: Duration and bandwidth of the chirp pulses used in a series of SPEN DOSY experiments to characterise the effect of the time-bandwidth product while changing it.

Exp label	T_e (ms)	BW (kHz)	G_e (G/cm)
1	1.0	55	13.0
2	1.5	55	13.0
3	2.0	55	13.0
4	2,5	55	13.0
5	3.0	55	13.0
6	3,5	55	13.0
7	4.0	55	13.0
8	4,5	55	13.0
9	5.0	55	13.0

Table 3: Comparison of the signal-to-noise ratio between conventional and SPEN experiments for DOSY experiments on mixture M1. The conventional experiment was carried out with a restricted sample length of 10 mm while the SPEN experiment was carried out with a classical tube, with a chirp sweeping on 10mm. The acquisition duration for both experiments was about 35 minutes.

Molecule	Peak number	SNR_{conv}/SNR_{SPEN}
Caffeine	1	6.3
	4	5.8
	5	5.8
	7	5.8
Ethyl Acetate	3	6.6
	9	6.2
	10	6.7
DMSO	8	4.3
Methanol	6	4.1
HDO	2	2.8

Graphical abstract

Optimisation of spatially encoded diffusion ordered NMR spectroscopy
for the analysis of mixtures

Corentin Jacquemmoz, Rituraj Mishra, Ludmilla Guduff, Carine van Heijenoort, Jean-Nicolas Dumez*

Spatially-encoded (SPEN) diffusion-ordered NMR spectroscopy (DOSY) is a fast method to correlate NMR information and translational molecular diffusion, with potential applications to the analysis of mixtures. Until now, the method has only been briefly described. Here we provide a thorough descriptions of its features, demonstrated with experiments, that will be useful for the implementation and optimal use of the method.